







Visual Soil Structure Quality Is Mostly Explained by Small-Size Structural Pores

¹University of Applied Sciences of Western Switzerland, HES-SO, Hepia-inTNP, Soils and Substrates Group, Geneva, Switzerland | ²Department of Environmental Systems Science, ETH, Soil Resources Group, Zürich, Switzerland | ³Department of Environmental Systems Science, ETHZ, Sustainable Agroecosystems Group, Zürich, Switzerland | ⁴Natural Resources & Agriculture, Agroscope, Zürich, Switzerland | ⁵Swedish University of Agricultural Sciences, Soil & Environment, Uppsala, Sweden

Correspondence: Cédric Deluz (cedric.deluz@hesge.ch)

Received: 16 May 2025 | Revised: 2 October 2025 | Accepted: 7 October 2025

Funding: This work was supported by Swiss Federal Office for Agriculture, Grant/Award Number: 77a project Terres Vivantes; Swiss Federal Office for Environment, Grant/Award Number: BiodivSol project.

Keywords: carbonate | CoreVESS | shrinkage curve analysis | small-size structural pore | SOC | SOC:clay ratio | soil structure | structure quality

ABSTRACT

Visual assessment of soil structure receives growing interest but its physical meaning is still to be explored. This study examined the relationships between soil pore systems volume and size distribution and visual structure quality scores in undisturbed soil samples from Swiss cropland soils covering a wide range of soil organic carbon (SOC) and clay contents. Structure quality scores were determined with CoreVESS. The pore system volumes were quantified by shrinkage analysis, and the water retention curves were used to determine the equivalent pore-size distribution. CoreVESS scores showed non-linear relationships with total and structural pore volumes. They correlated mainly to structural porosity volume, whereas plasma pores did not explain structure quality scores. As a result, the total porosity was less correlated to CoreVESS than structural porosity. The small-size (<50–100 µm equivalent diameter) structural pore volume showed the higher correlation to structure quality score. The small-size structural pore volume was mostly correlated with the SOC:clay ratio and, to a lesser extent, with SOC, highlighting the link between soil structure quality and clay-SOC complexation in these soils. Soils with SOC:clay ratios above 0.1 showed significantly larger volumes of small structural pores. Our findings underline the functional importance of these small-size structural pores, which are also accounting for air-water equilibrium close to field capacity, and were pointed out for their role as soil biota habitat. Their tight relationship with SOC suggests a good stability upon stresses and slow changes over time. In contrast, large structural pores, which are known to be sensitive to mechanical stress of soil fauna activity, were primarily influenced by carbonate content.

1 | Introduction

Soil structure is a cornerstone of soil fertility, which is often in critical condition on arable land. Assessing and restoring soil quality have become key objectives (Lal 2015; Bünemann et al. 2018). Despite considerable efforts, defining soil structure quality using physical measurements either focused on the voids (soil pores) or the solids (aggregates) largely failed (Horn and Fleige 2003; Alaoui et al. 2011; Rabot et al. 2018), thus jeopardising the adoption and application of indicators of soil

Abbreviations: CoreVESS, visual evaluation of soil structure performed on a standardised matric potential soil core; SOC, soil organic carbon; SOM, soil organic matter; VESS, visual evaluation of soil structure; V_p , Total porosity [cm³g⁻¹]; V_{pl} , Plasma porosity [cm³g⁻¹]; V_{Str} , Structural porosity [cm³g⁻¹]; W, Gravimetric water content [gg⁻¹].

This is an open access article under the terms of the Creative Commons Attribution License, which permits use, distribution and reproduction in any medium, provided the original work is properly cited.

© 2025 The Author(s). European Journal of Soil Science published by John Wiley & Sons Ltd on behalf of British Society of Soil Science.

Summary

- Structure quality was better correlated to structural porosity than total porosity.
- Small (<100 µm equivalent eqØ) structural pores correlate best with structure quality.
- Small structural pores are mostly correlated to organic carbon to clay ratio.
- These pores are key to structure quality and air-water equilibrium.

physical quality. Simple parameters (e.g., bulk density or penetrometer measurements) provide only limited interpretative insight, while performing multiple physical determinations is technically demanding and expensive. Moreover, physical parameters exhibit large spatial variability and unstable variances with measurement device size (Nielsen et al. 1973; Sisson and Wierenga 1981; Vauclin et al. 1982). Due to these difficulties, defining soil structure quality based on physical measurements is still to be achieved.

A single parameter such as total porosity or saturated hydraulic conductivity fails to capture the structure quality, which integrates among others the pore volumes and size distribution, the pore network architecture, and the soil mechanical stability. Moreover, the pore network architecture and volume are highly dynamic with time and water content, due to shrink swell processes, particularly in soils containing swelling clay (Bronswijk 1991; Boivin et al. 2009; Coppola et al. 2015; Bottinelli et al. 2016). Shrinkage is controlled by different soil properties (Boivin 2023) such as clay content and clay type (Boivin et al. 2004), and by external stresses (e.g., Schäffer et al. 2008; Goutal-Pousse et al. 2016). Various classifications of soil pores, based on size classes (Perret et al. 1999), origin, shape (Brewer 1964) and functional properties (Gerke and Van Genuchten 1993; Boivin et al. 2004) have been proposed (Schäffer et al. 2013). Soil porosity, however, was long ago recognised as physically organised in two distinct pore systems with distinct origin and functions, namely structural and plasma pores (Brewer 1964). These two pore systems were first defined by micromorphologists on thin sections observation (Verrecchia and Trombino 2021), and later quantified physically using shrinkage analysis (ShA) (Boivin 2023). Structural pores include cracks, biopores, and packing voids, and account for rapid transfers and air-water equilibrium in soils. The soil plasma is made of the soil colloids ("Glossary of Soil Science Terms | Soil Science Society of America," 2025), namely the clay minerals coated with organic matter and oxides, sometimes referred to as soil matrix or its porosity as textural porosity, though these concepts are not identical as discussed in Schäffer et al. (2013). Working at clod or core sample scale, shrinkage analysis (ShA) allowed to quantify the volume changes in these pore systems with water content, soil constituents, biological activity, and mechanical stress, as reviewed by Boivin (2023), thus providing a broad assessment of the soil physical properties.

Because of the limitations faced with physical characterisation of the soil structure, the evaluation of soil structure based on visual observation was long ago developed (Ball et al. 2007).

The Visual Evaluation of Soil Structure (VESS) spade test (Ball et al. 2017) received growing attention for its ability to quantify the soil physical quality of a topsoil block in a fast-operated and reliable way (Leopizzi et al. 2018). VESS uses simple visual criteria shared by the soil scientists to score the structure quality from 1 (very good) to 5 (degraded).

The relationships between physical parameters and the VESS score were first studied by Guimarães et al. (2013) on the VESS, and subsequently in more detail on a version adapted to the size of soil core samples (CoreVESS) (Johannes, Weisskopf, et al. 2017; Lin et al. 2022). The sequence of physical changes occurring in a soil sample with increasing soil structure quality CoreVESS score, that is, decreasing structure quality has been described as follows: loss of the coarser structural pores from CoreVESS score 1 to 2, continuous slow decay of structural porosity volume until CoreVESS 3, and collapse of the soil structure upon drying for larger CoreVESS (Johannes, Weisskopf, et al. 2017).

Linear relationships between soil organic carbon (SOC) concentration and physical parameters has been long ago recognised (e.g., Manrique and Jones 1991; Imhoff et al. 2004; Goutal-Pousse et al. 2016; Johannes, Matter, et al. 2017; Sauzet et al. 2024). Oppositely, Johannes, Matter, et al. (2017) showed a non-linear relationship between SOC and visual structure quality score. This latter was explained by the SOC:clay ratio, also referred to as clay saturation ratio, as early suggested by Dexter et al. (2008). The relationship between the structure quality scores and the SOC:clay ratio showed that the degree of clay saturation by organic matter allowed to determine the SOC:clay ratios thresholds of 0.08, 0.1 and 0.12 as the average values for CoreVESS scores ≥ 4 , <4 and >2, and ≤ 2 , respectively, that is, corresponding on average to degraded, fair and good observed structure quality in Swiss cropland soils, respectively (Johannes, Matter, et al. 2017). Since these SOC:clay ratios correspond to a probability of the structure to be degraded, good, or fair, respectively, the SOC:clay ratio was proposed as the soil structure vulnerability index by Fell et al. (2018) and Dupla et al. (2021). However, the mechanisms underpinning the relationship between visually scored soil structure quality, the soil components and its physical properties are still to be deciphered.

In this study, we analysed the relationship between pore size distribution, soil components, and soil structure quality to acquire better understanding of the significance of structure quality degradation. To this end, we quantified the pore properties and size distribution of undisturbed soil samples collected from Swiss arable land, with a wide range of SOC and clay content.

2 | Materials and Methods

2.1 | Study Area and Sampled Fields

Undisturbed topsoil samples were collected from 60 cropland fields, with field sizes ranging from 0.3–6 ha and an average of 2.6 ha. The selected fields, located in the Swiss plateau and Swiss Jura regions (Figure 1), were each previously described either in Johannes, Matter, et al. (2017), Dupla et al. (2022), Johannes et al. (2023), and Deluz et al. (2024).

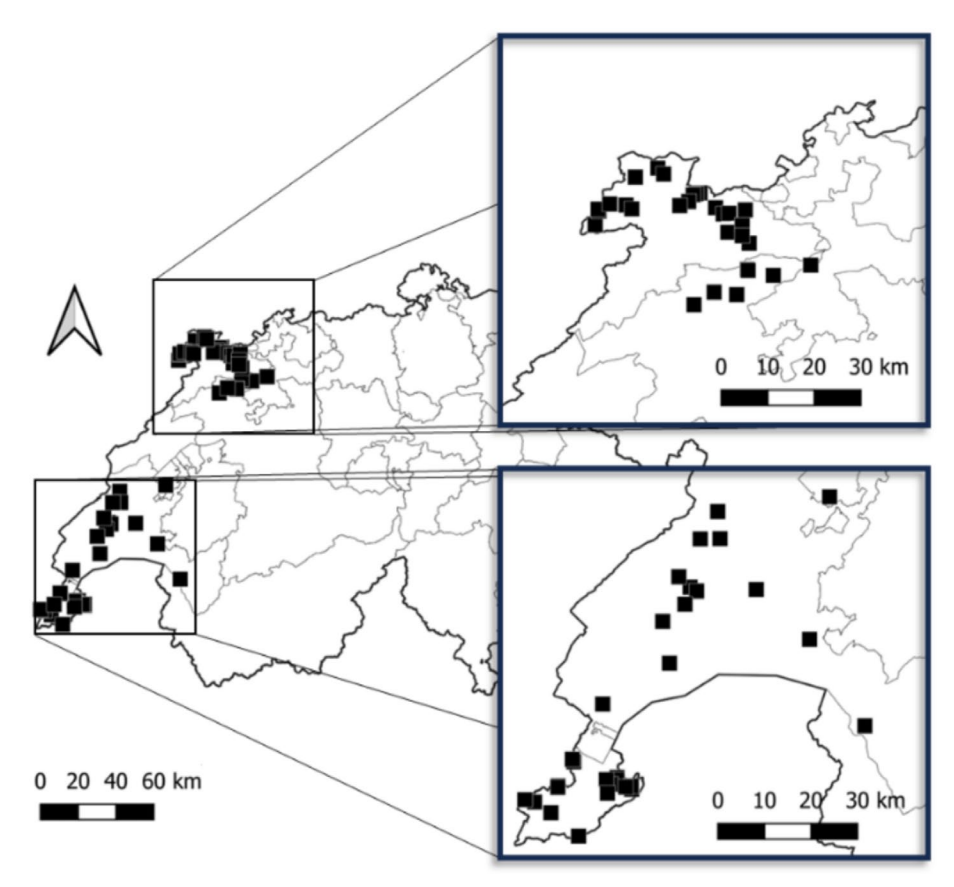


FIGURE 1 | Location of the 60 sampled fields on the map of Switzerland and its cantons. The two squares zoom in on the 30 sampled fields in the north-west (Jura and Bern) and the 30 sampled fields in the south-west (Leman region). All fields are located on Cambisol formed respectively on Jurassic limestone with occasional loess deposits and on Quaternary mixed carbonate moraines or Tertiary molasse.

TABLE 1 | Mean, median, standard deviation (SD), minimum and maximum values of the main characteristics of the sampled fields and farms on the undisturbed samples. Soil organic carbon content (SOC), texture (clay, silt, and sand content), carbonate content (CaCO $_3$), and pH (H $_2$ O).

Main soil parameter	Average	Median	SD	Min	Max
SOC [%]	2.9	2.6	1.4	1.0	7.0
Clay [%]	31.3	29.5	11.2	9.3	60.3
Silt [%]	43.7	41.7	10.8	19.3	66.5
Sand [%]	23.9	23.1	16.9	1.0	58.2
CaCO ₃ [%]	2.2	0.0	4.2	0.0	17.6
pН	6.6	6.8	0.6	5.2	7.6

Our selection aimed to encompass a wide range of soil organic carbon (SOC), clay content, pH, and limited carbonate content, as summarised in Table 1. SOC content ranged from 1.0%-7.0%, clay content ranged from 9.3%-60.3%, pH (measured in a $1/2.5~H_2O$ extract) ranged from 5.2-7.6, and carbonate content ranged from 0%-17.6%, though two-thirds of the soils contained no carbonates. Similar to the strategy applied in Johannes, Matter, et al. (2017), Dupla et al. (2022) and Deluz et al. (2024), a large range of cropping practices was

considered as well, from conventional tillage to no-till farming, with or without livestock and cover crops, with as uniform distribution of the practices among the fields as possible. Sampling was performed in spring before any soil tillage. All fields were classified as Cambisols according to the World Reference Base for Soil Resources (WRB 2022). The soils from the Swiss plateau are predominantly formed on mixed Quaternary carbonated moraine with some tertiary molasses. Their clay minerals are mostly inherited, of large size, with limited cation exchange capacity and mixed mineralogy (i.e., illite, vermiculite, and interstratified; personal data). The soils from the Jura region are primarily formed on Jurassic limestone containing smectite, illite and kaolinite, with occasional loess deposits. The average annual rainfall in the sampled regions ranged from 900-1100 mm, with average annual temperatures ranging from 10.1°C-14.0°C.

2.2 | Soil Sampling

Undisturbed soil core samples of approximately 125 cm³ were collected in spring 2021 from each field at 5–10 cm depth, before any soil tillage in the same year. Each sample was collected in duplicate at the centre of each field after a visual assessment to avoid wheel tracks or any noticeable soil disturbance. This sampling method was shown to provide samples with SOC and clay content well representative of the field SOC and clay content (Deluz et al. 2025) and duplicates were kept in case of structure

Sample preparation and measurement workflow

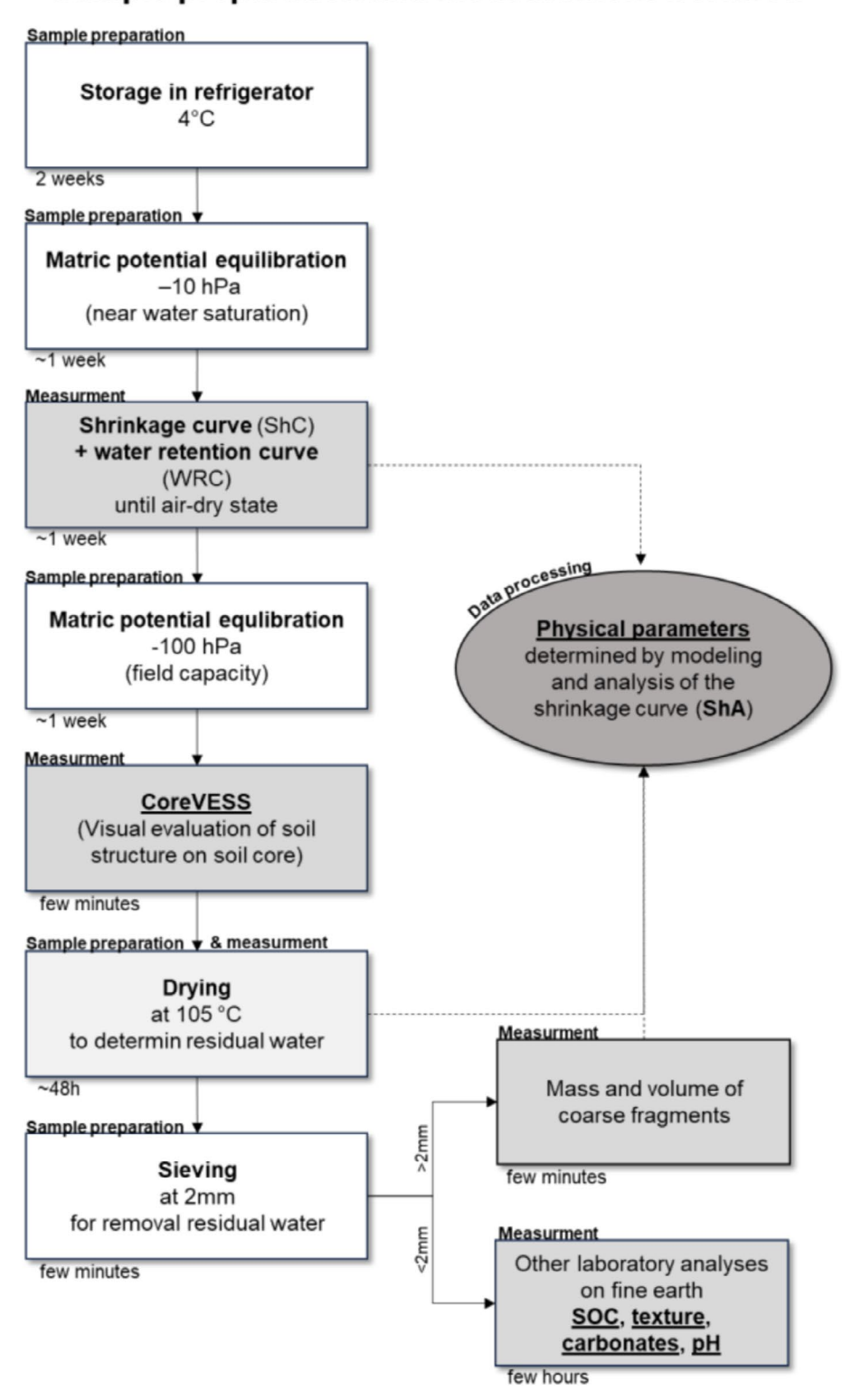


FIGURE 2 | Sketch of the sample preparation and measurement workflow. Solid arrows indicate the sequence of steps, dashed arrows represent the data flow required for shrinkage analysis (ShA) (grey circles). White boxes correspond to sample preparation steps, whereas grey boxes indicate measurement phases. The parameters obtained and used in this study are underlined.

damage of the main sample. We used the core sampler described by Johannes, Weisskopf, et al. (2017), which allowed us to perform quality control after sampling to check that the structure was not disturbed. The samples were placed in a sealed plastic

bag, transported in a cool box to the laboratory, and stored at 4°C for about 2 weeks before analysis. An overview of the sample preparation process, as well as the measurements performed and detailed in the following sections, is presented in Figure 2.

2.3 | Shrinkage Curve Measurement and Analysis

We followed the procedure described in for example, Schäffer et al. (2008) to determine the sample's shrinkage curves (ShCs). Briefly, the undisturbed soil cores were extracted from the cylinder and equilibrated at a matric potential of -10hPa in a sandbox without limitation of their swelling. The bulk volume of the swollen soil core was then measured using a 3D structured light scanner (EinScanSP scanner from SHINING 3D). The wet samples were then introduced in the shrinkage apparatus, where they were free to dry slowly while the changes in sample weight and height were recorded quasi-continuously, as described in Boivin et al. (2004). The water retention curve (WRC) was recorded simultaneously using a ceramic cup micro tensiometer inserted at the centre of the sample. When steady weight and volume were observed, the air-dried sample volume was measured and then dried at 105°C to remove residual water. The undisturbed samples were sieved to 2 mm to determine the coarse fraction (> 2 mm) volume and weight. The coarse fraction's weight and volume were then subtracted from the bulk volume and weight of the sample to calculate the bulk volume and weight of the fine earth (<2mm) after drying. The changes in sample height were converted into changes in sample volume after calculating the geometric factor based on the initial and final sample volume and height, respectively (Boivin 2007). The sample ShC was, therefore, represented as the specific (i.e., per unit of mass) volume V (cm³ g⁻¹) of the fine earth as a function of its gravimetric water content W (gg⁻¹).

The exponential (XP) model was then fitted to the experimental ShC for shrinkage analysis (ShA) as described in Schäffer et al. (2013). Briefly, the XP model assumes a dual pore system in the soil, corresponding to the structural and plasma pores (Boivin et al. 2004). Based on the assumed properties of these pore systems, the XP model allows to describe the ShC as a succession of linear shrinkage domains overlapping in curvilinear sections. Fitting the coordinates of the transition points between the linear and curvilinear sections allows calculating the structural and plasma pores volume, water content and air content at any soil water content. Moreover, the slopes of the linear domains, namely structural and basic shrinkage domains quantify the capacity of the pore structure to withstand drying forces (Schäffer et al. 2013) which can, therefore, be interpreted as the hydro-structural stability of the soil sample.

Based on these calculations, we obtained for each sample a series of physical parameters such as the slope of the structural shrinkage $K_{\rm Str}$, total pore specific volume $V_{\rm P}$ (cm³ g⁻¹), structural pores volume $V_{\rm Str}$ (cm³ g⁻¹), structural pores water content $W_{\rm Str}$ (g g⁻¹), plasma pores volume $V_{\rm Pl}$ (cm³ g⁻¹), plasma water content $W_{\rm Pl}$ (g g⁻¹), and sample specific air content Air (cm³ g⁻¹) as a function of the sample water content W (g g⁻¹). Since the pore volumes are changing upon shrinkage, the values can be taken at selected matric potentials, which was used in subscript. For instance, the specific air content at—100 hPa was denoted Air_100.

2.4 | Pore Volume According to Matric Potential and Equivalent Pore Size Classes

The $V_{\rm p}$, $V_{\rm Str}$, and $V_{\rm pl}$ volumes were calculated for different matric potential intervals. Each volume was equal to the change in

water content in the matric potential interval. The Jurin-Laplace law was used to estimate the equivalent pore size diameter (eq \emptyset) of the draining pores in the tensiometer range. We used the simplified equation:

$$d = 0.3/h \tag{1}$$

where d is the eqØ of the soil pores in cm and h is the absolute value of the matric potential in hPa (Jury and Horton 2004). The matric potential intervals were determined using a Fibonacci sequence, with the aim to obtain as a similar pore volume as possible across the different eqØ (matric potential) intervals. This resulted in 11 matric potential intervals from -1000 to -7 hPa, namely <-1000 hPa ($<3\mu$ m eqØ); -1000 to -500 hPa ($3-6\mu$ m); -500 to -333 hPa ($6-9\mu$ m); -333 to -200 hPa ($9-15\mu$ m); -200 to -125 hPa ($15-24\mu$ m); -125 to -77 hPa ($24-39\mu$ m); -77 to -48 hPa ($39-63\mu$ m); -48 to -29 hPa ($63-102\mu$ m); -29 to -18 hPa ($102-165\mu$ m); -18 to -11 hPa ($165-267\mu$ m) and -11 to -7 hPa ($267-432\mu$ m).

In the shrinkage model, plasma pores are assumed to remain water saturated in the tensiometer matric potential range, thus showing no air-water menisci. Therefore, we preferred not to apply the Jurin-Laplace law to these pores, and only matric potential intervals are reported for plasma pores in the following, while eq \emptyset range is mentioned together with matric potential range for structural pores.

2.5 | Sample Structure Quality: CoreVESS Score

CoreVESS allows us to visually score the structure quality from 1 to 5 according to three criteria: (i) breaking difficulty, (ii) aggregate shape, (iii) visible porosity. A score of 1 indicates excellent structure quality and a score of 5 indicates poor structure quality. The overall procedure for CoreVESS score determination followed the protocol determined in Johannes, Weisskopf, et al. (2017). After ShC measurement, the samples were re-equilibrated at a matric potential of $-100\,\mathrm{hPa}$ prior to visually assessing soil structure quality scores in double-blind conditions with two experienced assessors. The two independent scores were generally similar, and the average was considered in case of small divergence.

2.6 | Texture, Soil Organic Carbon and Other Soil Analyses

The samples were analysed for texture, SOC, and carbonate content. Soil texture (clay, silt and sand fractions) was determined by sedimentation (ISO 11277). Soil carbonates were measured using the gas-volumetric method analysis with the Bernard calcimeter (ISO 10693). Soil organic carbon was determined using the modified Walkley and Black (1934) (ISO 14235), corrected using the equation of Brogan (1966) to yield similar results as dry combustion, as validated by independent (ISO 17043) proficiency test.

2.7 | Data Analysis

Data analysis was conducted in two steps. In the first step, we explored the correlations between CoreVESS scores and physical parameters obtained from ShA at fixed matric potentials, which allowed us to determine the most discriminant physical parameters with respect to structure quality score. In the second step, we analysed the relationships between soil components, CoreVESS scores and pore volume split into classes of desorption matric potential intervals, to describe in detail the interplay between observed soil structure quality, soil components, pore types and pore size ranges.

Statistical analyses were conducted using R software (R Core Team (2020) version 3.6.1). The significance level considered was p < 0.05. When the assumptions of normality and homoscedasticity was not met, Spearman's rank correlation was used to select the physical parameters showing the strongest correlation with CoreVESS at fixed matric potential. On the selected parameters, principal component analysis (PCA) was then used to plot the relationships between the volumes of pores draining at the different matric potential intervals, the CoreVESS scores were used as labels and the centre of gravity of each CoreVESS score was plot. Since $V_{\scriptscriptstyle \mathrm{P}}$ range was large between the samples, the volumes were considered both in absolute values (cm³ g⁻¹) and in % of the sample total pore volume. The correlations between the different pore volume size classes and analytical soil properties (texture, carbonate, SOC, SOC:clay ratio) were analysed using a Spearman correlation matrix. The significance of the differences between correlations was discussed using Fisher's Z-tests (R package: cocor). Significant differences between groups were assessed using ANOVA tests followed by Tukey's post hoc tests (R package: stats). The Kruskal-Wallis test with Dunn's post hoc test was used in the case of non-parametric data (R package: dunn. test).

3 | Results

3.1 | Physical Parameters Correlated to CoreVESS Scores

The physical parameters showing the higher correlation to CoreVESS scores are those associated with structural porosity, such as $V_{\rm Str}$, $K_{\rm Str}$, and Air content, since in the tensiometric range only the structural pores allow air entry. The parameters related to plasma porosity volume were weakly correlated with CoreVESS scores, while total porosity volume, which combines plasma and structural porosities, showed intermediate correlations. The correlations were increasing with decreasing matric potential (e.g., $-1000\,{\rm hPa}$). Based on this preliminary analysis, we selected $K_{\rm Str}$, $V_{\rm Str-1000}$, ${\rm Air}_{-1000}$, $V_{\rm Pl-1000}$, and $V_{\rm P-1000}$ to further investigate their relationships with CoreVESS. The detailed correlation analysis is reported in the Supporting Information S1.

The relationships between CoreVESS scores and $K_{\rm Str}$, $V_{\rm P-1000}$, $V_{\rm Str-1000}$, $V_{\rm Pl-1000}$ and ${\rm Air}_{\rm -1000}$ are reported in Figure 3. Most relationships were not linear. $K_{\rm Str}$ was increasing with CoreVESS scores following a sigmoidal pattern. $K_{\rm Str}$ was nearly constant for CoreVESS scores below 2, with an average slope value of ~0.3. Then $K_{\rm Str}$ rapidly increased from CoreVESS 2 to 3.5 and remained nearly constant above 3.5, with an average slope value of 0.6. The mean slope value for score 3 was 0.5 (Figure 3A).

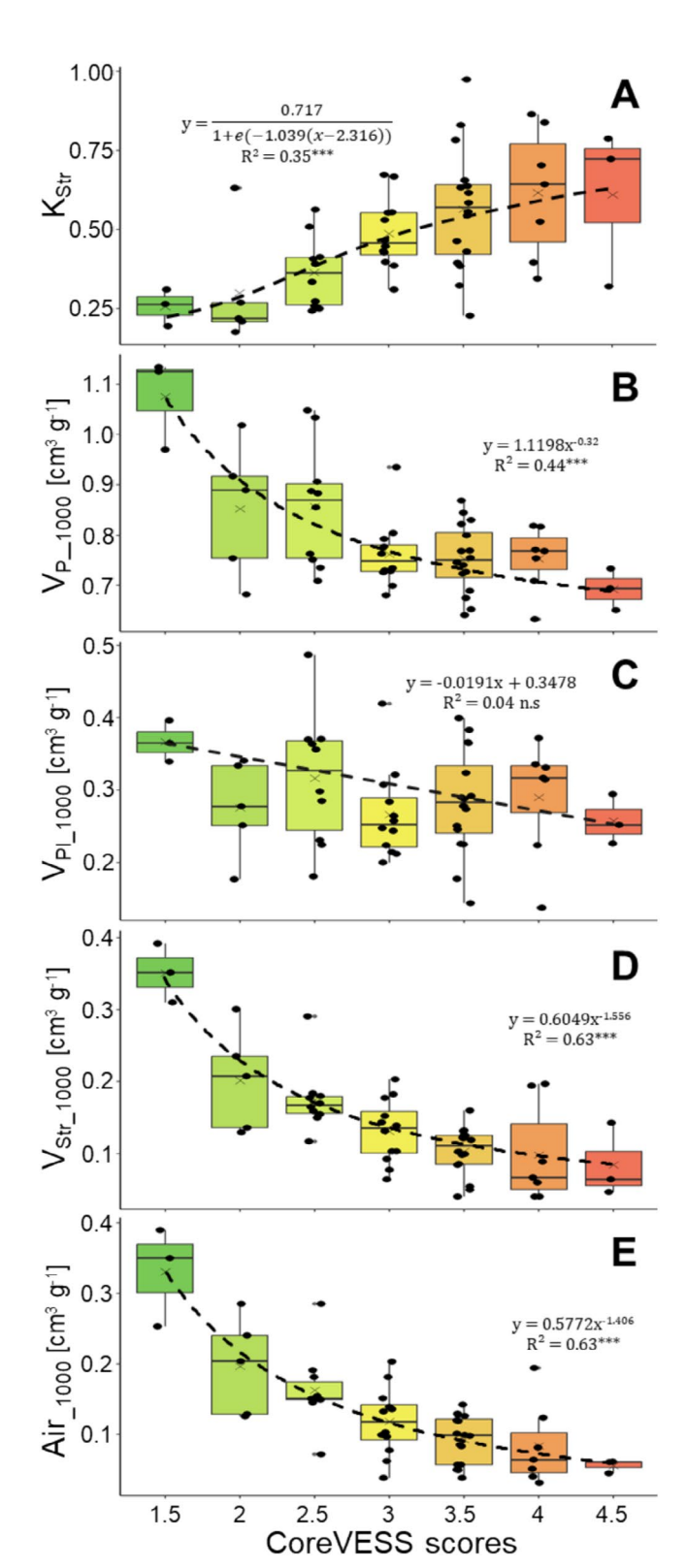


FIGURE 3 | Combined boxplot and scatterplot displaying: (A) structural slope ($K_{\rm Str}$), (B) specific pore volume ($V_{\rm P}$), (C) plasma porosity ($V_{\rm Pl}$), (D) structural porosity ($V_{\rm Str}$) and (E) gravimetric air content (Air) to a matric potential of pF3 ($-1000\,{\rm hPa}$) on the y-axis against CoveVESS scores on the x-axis. n.s and *** indicate not significant ($p_{\rm value} > 0.05$) and highly significative model ($p_{\rm value} < 0.001$), respectively.

The relationship between $V_{\rm p}$ and CoreVESS followed a negative power function, which was also observed for $V_{\rm Str}$ and Air, respectively. The coefficient of determination of the

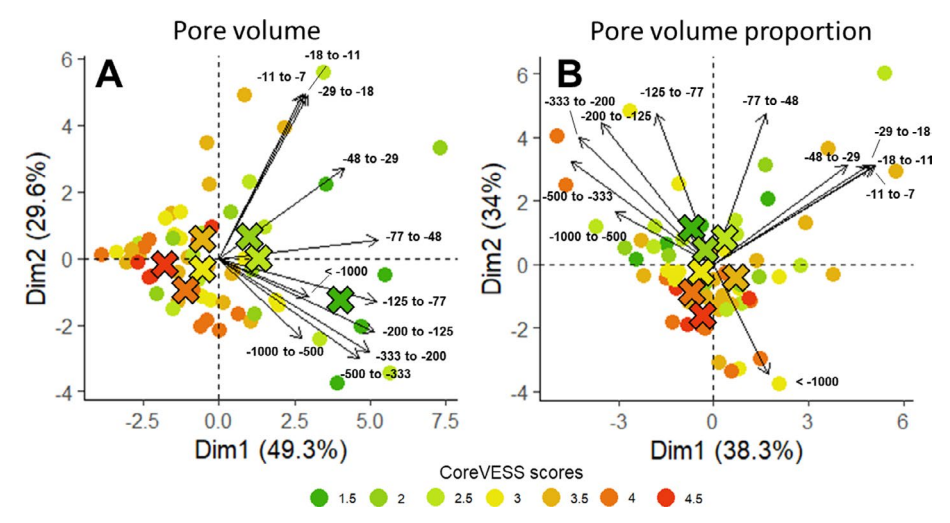


FIGURE 4 | PCA of the different pore volume matric potential classes, in absolute pore volume (A) or as a proportion of total pore volume (B). Observations are reported onto the PCA with colour code corresponding to the CoreVESS score. Large crosses represent the centroids' CoreVESS scores.

relationship was significantly higher for $V_{\rm Str}$ and Air (R^2 = 0.63 for both) than for $V_{\rm P}$ (R^2 = 0.44) according to Fisher's *Z*-test (Figure 3B,D,E).

 $V_{\rm Pl}$ decreased non-significantly with increasing CoreVESS with $V_{\rm Pl}$ ranging between ~0.25 and 0.4 cm³ g⁻¹ independently from the CoreVESS score (Figure 3C).

3.2 | Pore Size and CoreVESS Scores

The PCA of the pore volumes corresponding to the different matric potential classes is shown in Figure 4 with CoreVESS scores as labels, while the correlations between CoreVESS scores and the different matric potential classes are presented in Table 2. The PCA performed on absolute specific volume (cm 3 g $^{-1}$) values is reported in Figure 4A and on relative % of the total pore volume of the sample in Figure 4B. The first two components represented 78.9% and 72.3% of the data variance, respectively. The following observations can be made.

The pore volumes associated with the higher matric potentials (larger draining pores), namely > $-29\,hPa~(eq\oslash>102\,\mu m)$ in Figure 4A,B, respectively, are orthogonal to the pore volumes draining below $-77\,hPa~(eq\oslash<39\,\mu m)$ which suggests that the pore volumes of these two categories developed independently. The pore volumes associated with intermediate matric potential intervals were next to the bisector between these two categories.

Moreover, Figure 4B, showed that the proportion of pores draining between -1000 and $-48\,hPa$ (-3 to $-63\,\mu m$ eqØ) was inversely correlated to the proportion of pores draining below $-1000\,hPa$. This suggests that the two categories developed one at the expense of the other, which is consistent with micro-crack structural pores developing in the plasma porosity as assumed by shrinkage modelling.

The CoreVESS scores were generally decreasing (increasing structure quality) with increasing pore volume percentage of the

pores draining in the -77 to -1000 hPa matric potential interval (Figure 4B), with little contribution of the larger pores.

Almost all the $V_{\rm p}$ pore classes were correlated to CoreVESS scores except for the smallest matric potential range (< -1000 hPa) (Table 2). The $V_{\rm Str}$ of structural pores draining at matric potential higher than -125 hPa (> 24 μ m eq \varnothing) showed a higher correlation to CoreVESS scores than $V_{\rm p}$ pores, whereas only plasma pores draining in the lower matric potential range (< -1000 hPa) were more strongly correlated to CoreVESS than $V_{\rm p}$ pores of the same class. The higher correlation (r = 0.54) was observed for the -48 to -77 hPa class (24–39 μ m eq \varnothing), which primarily consists of structural pores (on average > 90%).

3.3 | Soil Components and Pore Volume Distribution

Table 2 reports the Spearman correlations between the main analytical properties of the soil (texture, total carbonates, SOC and SOC:clay ratio) and the $V_{\rm P}$, $V_{\rm Str}$ and $V_{\rm Pl}$ pore volumes split into draining matric potential classes with corresponding pore eq \varnothing . The average relative proportions of plasma and structural pore volumes in the total pore volume are reported in the first columns.

 $V_{\rm P}$ pores draining above $-48\,{\rm hPa}$ (>63 µm eqØ) were almost entirely composed of structural pores (>95%), while the pores draining below $-1000\,{\rm hPa}$ (<3 µm eqØ) were only plasma pores (>99%). An increasing proportion of plasma pores with decreasing matric potential can be observed below $-48\,{\rm hPa}$, which corresponds to the maximum swelling of the plasma (top left in Table 2).

SOC and SOC:clay were positively correlated to V_p pore classes draining below $-48\,h\text{Pa}$ (<63 μ m eqØ). Conversely, no correlation of SOC and SOC:clay with the volume of pores larger than 63 μ m eqØ was observed, but carbonates showed positive correlations with V_p only for pores draining at matric potential larger than $-48\,h\text{Pa}$ (>63 μ m eqØ). Unsurprisingly, clay

TABLE 2 | Spearman correlation between the different pore systems volumes (total = $V_{\rm p}$, structural = $V_{\rm Str}$, and plasma = $V_{\rm pl}$ porosity) at different matric potential classes (or pore size equivalent diameter) and soil components such as texture (clay, silt, sand), calcium carbonates (CaCO $_3$), soil organic carbon (SOC), SOC:clay ratio, and visual scores of structure quality (CoreVESS). At the top left, shades of grey distinguish structural porosity proportion (light grey) and plasma porosity proportion (dark grey) for each matric potential (or pore size) range. The darker the blue boxes, the more positively correlated the correlations, and the darker the red boxes, the more negatively correlated the correlations. Uncoloured correlations were not significant.

ighticant.														
	Pore system contribution [%]			Matric potential (absolute value) range and equivalent pore size diameter		SSE	Variables							
		Structural	Plasmia	SE	[hPa]	[μm Ø]	CoreVESS	Sand	Silt	Clay	CaCO ₃	SOC	SOC:clay	
_		100.0	0.0	0	7-11	432-267	-0.34	0.08	-0.14	-0.01	0.33	0.08	0.08	
		100.0	0.0	0	11-18	267-165	-0.35	-0.02	-0.09	0.09	0.30	0.11	-0.02	
	V_P [cm ³ g ⁻¹] Total porosity located at :	96.7	3.3	±1.3	18-29	165-102	-0.35	-0.05	-0.08	0.10	0.17	0.07	-0.05	
		94.6	5.4	±1.7	29-48	102-63	-0.36	-0.13	0.09	0.16	0.26	0.32	0.03	
		91.4	8.6	±2.6	48-77	63-39	-0.54	-0.12	-0.16	0.23	0.20	0.55	0.46	
	VP [cm ³ g ⁻¹]	75.9	24.1	±3.9	77-125	39-24	-0.42	-0.01	-0.26	0.17	0.00	0.60	0.63	
	[cr osit	49.6	50.4	±4.7	125-200	24-15	-0.39	-0.07	-0.29	0.26	0.02	0.66	0.61	
	V_{I}	26.3	73.7	±3.9	200-333	15-9	-0.37	-0.17	-0.20	0.32	0.02	0.66	0.53	
	otal	10.5	89.5	±2.7	333-500	9-6	-0.33	-0.15	-0.21	0.30	0.04	0.62	0.54	
	Ĭ	2.4	97.6	±1.1	500-1000	6-3	-0.17	-0.08	-0.20	0.18	-0.01	0.42	0.42	
		0.0	100.0	0	>1000	<3	-0.22	-0.59	0.29	0.62	0.07	0.82	0.34	
_					Tot	al	-0.37	-0.53	0.10	0.62	0.08	0.90	0.46	
				$\mathbf{V_{Str}} [\mathrm{cm}^3 \mathrm{g}^{-1}]$ Total porosity located at :										
					7-11	432-267	-0.34	0.08	-0.14	-0.01	0.33	0.08	0.08	
					11-18	267-165	-0.35	-0.02	-0.09	0.09	0.30	0.11	-0.02	
					18-29	165-102	-0.36	-0.04	-0.13	0.14	0.20	0.17	0.02	
					29-48	102-63	-0.39	-0.18	0.01	0.13	0.29	0.36	0.09	
					48-77	63-39	-0.53	0.05	-0.28	0.08	0.08	0.50	0.57	
				cm ³ ty l	77-125	39-24	-0.32	0.19	-0.41	0.00	-0.08	0.45	0.63	
				itr [(rosi	125-200	24-15	-0.13	0.16	-0.31	-0.03	-0.03	0.29	0.40	
				V s l po	200-333	15-9	-0.09	0.11	-0.21	-0.04	-0.02	0.18	0.27	
				ota	333-500	9-6	-0.07	0.07	-0.14	-0.01	0.04	0.20	0.25	
				L	500-1000	6-3	-0.04	0.14	-0.10	-0.09	0.08	0.14	0.19	
					>1000	<3	-	-	-	-	-	-	-	
					Total		-0.40	0.11	-0.33	0.04	0.04	0.41	0.49	
					7-11	-		-	-	-	-	-	-	
					11-18	-		-	-	-	-	-	-	
					18-29	-	-0.07	-0.20	0.18	0.14	0.13	-0.09	-0.29	
				ed a	29-48	-	0.00	-0.29	0.26	0.23	0.04	-0.04	-0.28	
				$V_{Pl}[cm^3\ g^{-l}]$ Total porosity located at :	48-77	-	-0.02	-0.41	0.33	0.35	0.18	-0.02	-0.41	
					77-125	-	-0.14	-0.29	0.20	0.27	0.14	0.06	-0.19	
			N N	osit	125-200	-	-0.27	-0.19	0.02	0.24	0.09	0.25	0.09	
				$V_{\rm F}$	200-333	-	-0.31	-0.23	-0.06	0.32	0.03	0.39	0.23	
			otal	333-500	-	-0.29	-0.21	-0.13	0.30	0.01	0.47	0.38		
				Ţ	500-1000	-	-0.29	-0.11	-0.18	0.27	0.05	0.48	0.52	
					>1000	-	-0.22	-0.59	0.29	0.62	0.07	0.82	0.34	
					Total		0.12	-0.58	0.19	0.63	0.09	0.87	0.42	
			•											

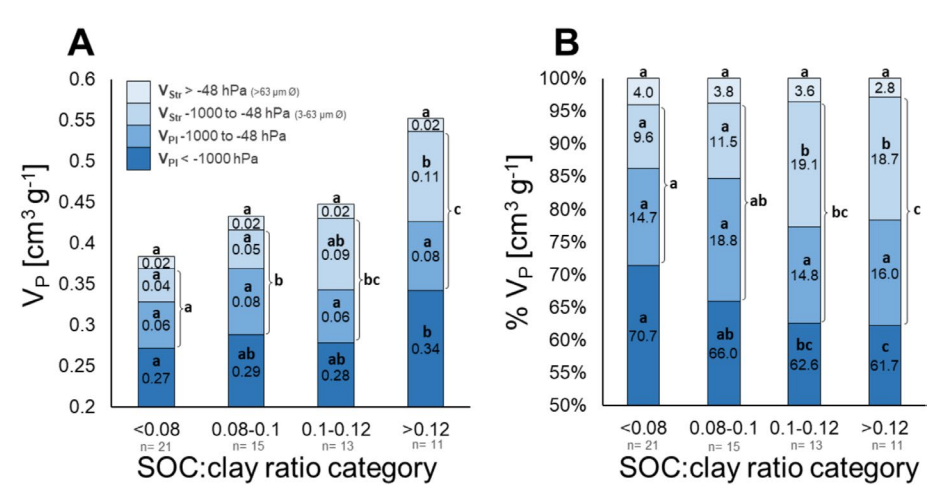


FIGURE 5 | Bar plot showing the soil porosity volume split into pore systems (structural and plasma) and size classes according to different SOC:clay ratio classes (<0.08; 0.08-0.1; 0.1-0.12; >0.12). Pore class volume is expressed in cm³ g⁻¹ (figure 7A) or as a relative percentage of total pore volume (figure 7B). $V_{\rm Str}>-48\,{\rm hPa}$ ($>63\,{\rm \mu m}$ eqØ) is represented in light blue, $V_{\rm Str}$ between $-1000\,{\rm and}\,-48\,{\rm hPa}$ ($3-63\,{\rm \mu m}$ eqØ) in medium blue, $V_{\rm Pl}$ between $-1000\,{\rm and}\,-48\,{\rm hPa}$ in blue, and $V_{\rm Pl}<-1000\,{\rm hPa}$ in dark blue. The scale starts at $0.15\,{\rm cm}^3\,{\rm g}^{-1}$ and 50% for graphs A and B, respectively. Letters indicate significant differences between pore class volumes in the Kruskal-Wallis followed by Wilcoxon test. $p_{\rm L}$ value <0.05.

and sand showed an opposing effect for V $_{\rm p}$ at matric potential below $-1000\,{\rm hPa}$ (< 3 $\mu{\rm m}$ eqØ) with positive correlation to clay, r=0.70) and negative correlation (sand, r=-0.65), respectively. Silts showed a negative correlation (r=<-0.29) to $V_{\rm p}$ pores draining below $-48\,{\rm hPa}$ (< 63 $\mu{\rm m}$ eqØ) and a positive correlation (r=0.26) to $V_{\rm p}$ pores draining at matric potentials lower than $-1000\,{\rm hPa}$ (< 3 $\mu{\rm m}$ eqØ) (top Table 2).

 $V_{\rm Str}$ pore volumes were positively correlated to SOC and SOC:clay ratio for all matric potential classes from $-48\,{\rm hPa}$ ($63\,{\rm \mu m}$ eqØ) to $-200\,{\rm hPa}$ ($15\,{\rm \mu m}$ eqØ) for SOC and to $-500\,{\rm hPa}$ ($6\,{\rm \mu m}$ eqØ) for SOC:clay, respectively. $V_{\rm Str}$ classes showed higher correlation with SOC:clay than with SOC, the correlations were not significantly smaller than for $V_{\rm p}$ and tended to decrease with decreasing matric potential. The same correlation trends as for $V_{\rm p}$ were observed between $V_{\rm Str}$ and texture classes. $V_{\rm Str}$ of pores draining at matric potential larger than $-48\,{\rm hPa}$ (> $63\,{\rm \mu m}$ eqØ) was positively correlated to carbonates similar to $V_{\rm p}$, which was logical since $V_{\rm Str}$ and $V_{\rm p}$ draining pores are identical in this pore-size range. The correlation between the > $63\,{\rm \mu m}$ eqØ structural pore volume and carbonates was significantly higher (R^2 =0.8) when only samples with carbonates were considered (Supporting Information S2).

For $V_{\rm Pl}$ pores draining below $-1000\,{\rm hPa}$, the correlation between $V_{\rm Pl}$ and clay was positive (r=0.62) and negative with sand (r=-0.59). $V_{\rm Pl}$ was strongly correlated to SOC for pores draining below $-1000\,{\rm hPa}$ (r=0.82), while the SOC:clay ratio was negatively correlated to $V_{\rm Pl}$ pores draining above $-125\,{\rm hPa}$, and positively correlated only for pores draining below $-500\,{\rm hPa}$ (bottom Table 2).

3.4 | Regrouped Pore Size Categories

In order to synthetize our results, we regrouped the pore system volumes into 4 categories based on the correlations (Table 2) and the PCA (Figure 4). Structural pore volumes were split into two categories, namely draining at matric

potential larger or smaller than -48 hPa, that is, correlated to carbonates (larger structural pores) or to SOC and clay (smaller structural pores), respectively. Plasma pore volumes were split into pores draining at larger matric potential than -1000 hPa (strongly correlated to SOC and clay), and smaller than -1000 hPa, respectively, owing to the distinct behaviour of these pores in the PCA (Figure 4B).

The relationship between the volumes of these pore categories and SOC, clay and SOC:clay were linear (Supporting Information S3). Our dataset showed the same SOC:clay categories as determined by Johannes, Matter, et al. (2017), namely SOC:clay ratios of 0.08, 0.10, and 0.12 departing the damaged, fair and good structure quality, respectively (Supporting Information S4). We summarised in Figure 5 the effect of increasing SOC:clay category on the volumes of the regrouped pore class categories. Figure 5A presents the absolute pore volumes and Figure 5B the pore volumes relative to total sample pore volume. The plasma pore volumes $(V_{\rm pl}\!<\!-1000\,{\rm hPa}$ and $V_{\rm Pl}$ between -1000 and $-48\,\rm hPa)$ remained unaffected by SOC:clay ratio while the structural pore volume V_{Str} draining between -1000 and $-48\,hPa$ (3-63 μm eqØ) showed the largest volume increase with SOC:clay (Figure 5A). In relative volumes, a non-significant decrease of $V_{\rm Str} > -48\,{\rm hPa}$ (>63 μm eqØ) with increasing SOC:clay was observed. The $V_{\rm pl}$ pore draining below -1000 hPa category decreased with increasing SOC:clay ratio. The proportion of V_{Str} pore draining between -1000 and -48 hPa (3-63 µm eqØ) showed almost a twofold increase for SOC:clay ratio higher than 0.1 (Figure 5B).

4 | Discussion

4.1 | Physical Properties and Structure Quality Visual Scores

First, our study confirms the previous results from Johannes et al. (2019) over an almost twofold higher range of SOC and clay contents (1% to 7% SOC and 9.3% to 60.3% clay content). We

observed that CoreVESS scores correlated with structural porosity volume rather than plasma pore volume at fixed matric potential (Figure 3). Our study confirms the other findings of Johannes, Weisskopf, et al. (2017), namely between scores 1 and 2 the soil structure quality decrease is associated with a sharp decrease of the large size (> 300 μm eqØ) structural porosity volume, then the $< 300 \,\mu m$ eqØ structural pore volume decreases until score 3 followed by a limited decrease above score 3, and a decrease of the hydro-structural stability (steeper slope of the shrinkage curve) corresponding to a collapse of the sample upon drying for scores higher than 3. Our main findings, however, are that we closely identified the determinants of soil structure quality: (i) the contribution of pore classes, particularly structural pores, to CoreVESS scores, and (ii) their interplay with SOC, clay, and carbonate contents.

4.2 | Contribution of Pore Classes to CoreVESS Structure Quality Scores

Analysing the contribution of V_{Str} eq \varnothing pore size classes to CoreVESS scores, gives a more detailed picture of the sample structure quality. The structural pores from 39 to $63\,\mu m$ eq \varnothing (draining between -77 and $-48\,hPa$), showed significantly better correlation with structure quality scores than total pore volume (Table 2). Though almost not visible with the naked eyes, the volume of these small-size structural pores is, therefore, closely linked to visual structure quality scores. Figure 4 further confirms this analysis by underlining the discriminant role of the small-size porosity volume. Note that the $<63\,\mu m$ eq \varnothing limit results from our method to split the pore volume into matric potential classes. Therefore, this value only reflects the importance of the small-size structural pores, smaller than 50 to $100\,\mu m$ eq \varnothing .

The structure is defined as the spatial organisation of the particles and pores of the soil (Warkentin 2008). It is thus susceptible to show rapid changes from second upon mechanical strains (Schäffer et al. 2013) to season upon resilience processes (Fell et al. 2018). The sharp decrease of the larger structural pores from scores 1 to 2 is accordant with the higher susceptibility to compaction of large pores (Alaoui et al. 2011), and the rapid creation of large pores by biological activity and cracking (Diel et al. 2019). However, the higher determined relationships between small-size structural pores and CoreVESS scores, on one hand, and SOC:clay and SOC on the other hand, suggests a specific role of these pores in structure quality. Because they are highly correlated to SOC, these pores should be more persistent in the soils than the larger pores and could play a major role in soil structure resistance and resilience. The higher correlation observed with SOC:clay accords with the concept of SOC complexation on clay and its significance for soil structure quality (Dexter et al. 2008; Johannes, Matter, et al. 2017; Prout et al. 2020).

4.3 | Soil Components and Soil Porosity

The general observation that SOC and to a lower extent clay are the main drivers of total $V_{\rm p}$ are nuanced when looking at pore size classes and pore systems (Table 2). The plasma pores volumes are largely explained by SOC and clay contents, which

is consistent with the role of these components in forming the plasma (Boivin et al. 2004, 2009), and with the positive influence of SOC content on plasma swelling as acknowledged by Schäffer et al. (2008) and Boivin et al. (2009).

The larger structural pores were correlated to the total carbonate content (Table 2 and Supporting Information S2). Falsone et al. (2010), Rowley et al. (2017) and the review of Virto et al. (2018) indicate that carbonates act as structure binding agents, promoting the formation of macro-aggregates through calcification processes, whereas organic matter and clays favour micro-aggregation. Carbonates, however, were present only in one-third of the samples (n=22). Carbonates can be in different forms, as primary particles or secondary precipitated particles. Their role on soil pore systems is, therefore, complex and remains to be deciphered. The absence of correlation between the volume of the larger pores and clay and SOC could be related to the higher variability of larger pores with time. They are preferentially destroyed upon mechanical strain or rapidly created with tillage and biological activity, thus limiting the effect of clay and SOC (Alaoui et al. 2011; Schäffer et al. 2013; Deluz et al. 2025).

4.4 | Significance of the Results

We first remind that our study includes a large range of cropping practices. These practices may impact factors of structuration in different ways and on different time scales, for example, by influencing SOC on the long range, or coarse porosity with tillage in the short range. By covering a large range of situations, we assume that the main relationships we observe between soil physical properties, structure quality and soil components, are not dependent of a particular cropping-practice such as no-till farming.

A second observation is that our results were obtained on Cambisols showing at least 9% clay content. Their clay content and mineralogy allowed to form a structure with aggregates and for ShCs, and, therefore, structural porosity, to be determined. Moreover, the SOC content of these soils is clearly determined by SOC complexation and protection on clay surfaces (Johannes, Matter, et al. 2017; Johannes et al. 2023; Deluz et al. 2024), thus showing a proportionality between SOC and clay, or clay + fine silt (Hassink 1997), which is not expected in for example, Andosols or chalk soils where SOC is protected by alternative mechanisms (Basile-Doelsch et al. 2007; Shabtai et al. 2023; Sauzet et al. 2024). Our conclusions should not be, therefore, applied to these soils.

According to our results, the total pore volume (or bulk density) is not a relevant indicator of structure quality. Though often used in that purpose (e.g., Poeplau and Don (2023) and Rabot et al. (2024)), it combines structural pores and plasma pores volumes which exhibit distinct relationships to SOC and clay content. The plasma pore volume, that can represent the major pore volume in clayey soils, mostly depend on clay content and to a lesser extent of SOC content rather than structure quality (Boivin et al. 2004; Schäffer et al. 2008; Goutal-Pousse et al. 2016). Therefore, this part of the soil porosity should not be considered in soil structure quality assessment.

While confirming the findings of Johannes, Weisskopf, et al. (2017), our study highlights a particular role for the small-size (<50–100 μm eqØ) structural pores in determining the visual score of structure quality. Less sensitive to mechanical impacts than the larger pores, these small-size structural pores were pointed out as a critical size range for easily available water (Zangiabadi et al. 2020), microbial activity and carbon sequestration (Kohler-Milleret et al. 2013; Kravchenko et al. 2019; Yudina and Kuzyakov 2023). In our study, their volume is highly correlated to SOC:clay and SOC, thus to components showing no changes (clay), or slow changes with time (SOC). The finding that the small-size structural pore volume is mostly determined by SOC:clay, namely the relative saturation of clay surfaces by SOC, while other pore categories are mainly proportional to SOC content, accord with the findings of Dexter et al. (2008), Johannes, Matter, et al. (2017) and Prout et al. (2020). Altogether, these studies strongly suggest that this pore-size category is a key feature for soil physical and biological quality and may allow to better understand structure vulnerability and improve structure quality management. These small-size structural pores probably provide the connection between coarser pores, which ensure rapid transfer of water and air, and the plasma pores that serve as a buffer for water and nutrients. Their role as habitat for biota is therefore critical. They can be regarded both as a determinant and an outcome of high structural quality, consistent with the self-organisation concept of the soil-plant-microbe system, which emphasises the mutual co-evolution of soil structure and biological activity, rather than a simple one-way causal relationship (Young and Crawford 2004; Kohler-Milleret et al. 2013). Despite their limited significance in terms of structure quality, the larger structural pores are important to allow transfers of water and air and root development in the soil when the structure was degraded. With that regard, a degraded structure score (3 and more) mostly indicates the loss of biota habitat in terms of food (SOC) and air-water equilibrium. While creating large pores may be a trigger of structure regeneration, only a SOC:clay larger than 0.1 would secure a minimum successful regeneration.

Determining the structural pore size distribution requires sophisticated equipment and cannot, therefore, become a routine indicator of structure quality, contrary to SOC:clay, provided that the threshold values of SOC:clay were shown to apply in the considered soil. Moreover, SOC:clay is an indicator of structure vulnerability, that is, of the probability to show a given structure quality across time and rotation (Sauzet et al. 2024), therefore it is an indirect indicator of the structure quality. A physical alternative is to determine the Air content, which is a close estimator of structural porosity as used by Johannes et al. (2019) in the soil structure degradation index. Therefore, the difference between air content at -50 and $-1000\,\mathrm{hPa}$ would be a good and easy to determine indicator of the small-size structural pore volume.

5 | Conclusions

This study allows to highlight the key role of small-size structural pores as determinants of soil structure quality. We first confirmed, on a broader range of clay and SOC content, the conclusions of Johannes, Weisskopf, et al. (2017) on the relationships

between visually assessed soil structure quality and pore system volumes as determined with shrinkage analysis. The degradation scheme proposed by Johannes, Weisskopf, et al. (2017) remains valid, with a successive loss of larger structural pores, followed by smaller ones, and, for highly degraded structures (visual score > 3), collapse upon drying.

Considering equivalent diameter categories (or matric potential intervals) in the pore systems revealed the close links between the volume of the small-size structural pores and a good structure quality, and the relationships between structural pore volumes and soil components. While SOC was the main determinant of the total porosity, the small-size structural porosity was more sensitive to the SOC:clay ratio, which suggests a key role of clay saturation by SOC in determining the structure quality, and, therefore, a better stability with time of the corresponding pores compared to large structural pores. These observations are consistent with previous research highlighting the key role of these pores for biological activity and in providing air-water equilibrium in soils. Altogether, these results strongly suggest that a good development of the small-size structural porosity is key to structure quality of soils. The correlations observed between carbonates and the coarsest pores call for further research on the role of carbonates on soil porosity, which is poorly documented.

Author Contributions

Cédric Deluz: conceptualization, investigation, writing – original draft, methodology, visualization, writing – review and editing, formal analysis, software, data curation. **Alyssa Deluz:** methodology, validation, formal analysis, conceptualization, software. **Thomas Keller:** supervision, writing – review and editing, validation. **Sebastian Doetterl:** supervision, writing – review and editing, validation, project administration. **Pascal Boivin:** supervision, resources, validation, writing – review and editing, project administration, funding acquisition.

Acknowledgements

The authors would like to warmly thank Aline Chambettaz and Sylvain Mischler from Hepia's Soil and Substrate Laboratory for their careful work on SOC and texture analyses. They are also grateful to the Swiss Federal Office for Agriculture (FOAG) for supporting Cédric Deluz's PhD through the 77 a-resources project "Terres Vivantes," and to the Swiss Federal Office for the Environment (FOEN) for additional support via the BiodivSol project. Finally, heartfelt thanks go to all the farmers who generously opened their fields and shared their time and local knowledge.

Conflicts of Interest

The authors declare no conflicts of interest.

Data Availability Statement

The data that support the findings of this study are available from the corresponding author upon reasonable request.

References

Alaoui, A., J. Lipiec, and H. H. Gerke. 2011. "A Review of the Changes in the Soil Pore System due to Soil Deformation: A Hydrodynamic Perspective." *Soil and Tillage Research* 115, no. 16: 1–15.

- Ball, B. C., T. Batey, and L. J. Munkholm. 2007. "Field Assessment of Soil Structural Quality A Development of the Peerlkamp Test." *Soil Use and Management* 23: 329–337.
- Ball, B. C., R. M. L. Guimarães, J. M. Cloy, P. R. Hargreaves, T. G. Shepherd, and B. M. McKenzie. 2017. "Visual Soil Evaluation: A Summary of Some Applications and Potential Developments for Agriculture." *Soil and Tillage Research* 173: 114–124.
- Basile-Doelsch, I., R. Amundson, W. E. E. Stone, et al. 2007. "Mineral Control of Carbon Pools in a Volcanic Soil Horizon." *Geoderma* 137: 477–489.
- Boivin, P. 2007. "Anisotropy, Cracking, and Shrinkage of Vertisol Samples. Experimental Study and Shrinkage Modeling." *Geoderma* 138: 25–38.
- Boivin, P. 2023. "Shrink-Swell Processes in Soils." In *Encyclopedia of Soils in the Environment*, 139–145. Elsevier.
- Boivin, P., P. Garnier, and D. Tessier. 2004. "Relationship Between Clay Content, Clay Type and Shrinkage Properties of Soil Samples." *Soil Science Society of America Journal* 68: 1145–1153.
- Boivin, P., B. Schaeffer, and W. Sturmy. 2009. "Quantifying the Relationship Between Soil Organic Carbon and Soil Physical Properties Using Shrinkage Modelling." *European Journal of Soil Science* 60: 265–275.
- Bottinelli, N., H. Zhou, P. Boivin, et al. 2016. "Macropores Generated During Shrinkage in Two Paddy Soils Using X-Ray Micro-Computed Tomography." *Geoderma* 265: 78–86.
- Brewer, R. 1964. Fabric and Mineral Analysis of Soils. John Wiley and Sons.
- Brogan, J. C. 1966. "Organic Carbon in Irish Pasture Soils." *Irish journal of agricultural research* 5: 169–176.
- Bronswijk, J. J. B. 1991. Measurement, Magnitude and Prediction of Field Swelling and Shrinkage. NATO ARW, Cornell University, 1–4.
- Bünemann, E. K., G. Bongiorno, Z. Bai, et al. 2018. "Soil Quality A Critical Review." *Soil Biology and Biochemistry* 120: 105–125.
- Coppola, A., A. Comegna, G. Dragonetti, H. H. Gerke, and A. Basile. 2015. "Simulated Preferential Water Flow and Solute Transport in Shrinking Soils." *Vadose Zone Journal* 14: vzj2015.02.0021.
- Deluz, C., A. Deluz, T. Keller, S. Doetterl, and P. Boivin. 2025. "Shrinkage Analysis of Repacked Soil Samples Enables Quantifying the Soil's Potential Physical Quality." *Soil Science Society of America Journal* 89: e70033.
- Deluz, C., D. Sebag, E. Verrecchia, and P. Boivin. 2024. "Soil Organic Matter Thermal Pools as Influenced by Depth, Tillage, and Soil Texture A Rock-Eval Analysis Study on the Cropland Soils of the Swiss Plateau." *Geoderma* 445: 116871.
- Dexter, A. R., G. Richard, D. Arrouays, E. A. Czyż, C. Jolivet, and O. Duval. 2008. "Complexed Organic Matter Controls Soil Physical Properties." *Geoderma* 144: 620–627.
- Diel, J., H.-J. Vogel, and S. Schlüter. 2019. "Impact of Wetting and Drying Cycles on Soil Structure Dynamics." *Geoderma* 345: 63–71.
- Dupla, X., K. Gondret, O. Sauzet, E. Verrecchia, and P. Boivin. 2021. "Changes in Topsoil Organic Carbon Content in the Swiss Leman Region Cropland From 1993 to Present. Insights From Large Scale On-Farm Study." *Geoderma* 400: 115–125.
- Dupla, X., T. Lemaître, S. Grand, et al. 2022. "On-Farm Relationships Between Agricultural Practices and Annual Changes in Organic Carbon Content at a Regional Scale." *Frontiers in Environmental Science* 10: 834055
- Falsone, G., M. Catoni, and E. Bonifacio. 2010. Falsoneetal._2010_res. pdf. Università di Torino DIVAPRA Chimica Agraria e Pedologia.

- Fell, V., A. Matter, T. Keller, and P. Boivin. 2018. "Patterns and Factors of Soil Structure Recovery as Revealed From a Tillage and Cover-Crop Experiment in a Compacted Orchard." *Frontiers in Environmental Science* 6: 134.
- Gerke, H. H., and M. T. Van Genuchten. 1993. "A Dual-Porosity Model for Simulating the Preferential Movement of Water and Solutes in Structured Porous Media." *Water Resources Research* 29: 305–319.
- Glossary of Soil Science Terms. 2025. Soil Science Society of America. https://www.soils.org/publications/soils-glossary?q=publications/soils-glossary/#.
- Goutal-Pousse, N., F. Lamy, J. Ranger, and P. Boivin. 2016. "Structural Damage and Recovery Determined by the Colloidal Constituents in Two Forest Soils Compacted by Heavy Traffic." *European Journal of Soil Science* 67: 160–172.
- Guimarães, R. M. L., B. C. Ball, C. A. Tormena, N. F. B. Giarola, and Á. P. Da Silva. 2013. "Relating Visual Evaluation of Soil Structure to Other Physical Properties in Soils of Contrasting Texture and Management." *Soil and Tillage Research* 127: 92–99.
- Hassink, J. 1997. "The Capacity of Soils to Preserve Organic C and N by Their Association With Clay and Silt Particles." *Plant and Soil* 191: 77–87.
- Horn, R., and H. Fleige. 2003. "A Method for Assessing the Impact of Load on Mechanical Stability and on Physical Properties of Soils." *Soil and Tillage Research* 73: 89–99.
- Imhoff, S., A. P. Da Silva, and D. Fallow. 2004. "Susceptibility to Compaction, Load Support Capacity and Soil Compressibility of Hapludox." *Soil Science Society of America Journal* 68: 17–24.
- Johannes, A., A. Matter, R. Schulin, P. Weisskopf, P. C. Baveye, and P. Boivin. 2017. "Optimal Organic Carbon Values for Soil Structure Quality of Arable Soils. Does Clay Content Matter?" *Geoderma* 302: 14–21.
- Johannes, A., O. Sauzet, A. Matter, and P. Boivin. 2023. "Soil Organic Carbon Content and Soil Structure Quality of Clayey Cropland Soils: A Large-Scale Study in the Swiss Jura Region." *Soil Use and Management* 39: 707–716.
- Johannes, A., P. Weisskopf, R. Schulin, and P. Boivin. 2017. "To What Extent Do Physical Measurements Match With Visual Evaluation of Soil Structure?" *Soil and Tillage Research* 173: 24–32.
- Johannes, A., P. Weisskopf, R. Schulin, and P. Boivin. 2019. "Soil Structure Quality Indicators and Their Limit Values." *Ecological Indicators* 104: 686–694.
- Jury, W., and R. Horton. 2004. Soil Physics. 6th ed. Wiley.
- Kohler-Milleret, R., R.-C. L. Bayon, C. Chenu, J.-M. Gobat, and P. Boivin. 2013. "Impact of Two Root Systems, Earthworms and Mycorrhizae on the Physical Properties of an Unstable Silt Loam Luvisol and Plant Production." *Plant and Soil* 370: 251–265.
- Kravchenko, A. N., A. K. Guber, B. S. Razavi, et al. 2019. "Microbial Spatial Footprint as a Driver of Soil Carbon Stabilization." *Nature Communications* 10: 1038. http://www.nature.com/articles/s41467-019-11057-4.
- Lal, R. 2015. "Restoring Soil Quality to Mitigate Soil Degradation." *Sustainability* 7: 5875–5895.
- Leopizzi, S., K. Gondret, and P. Boivin. 2018. "Spatial Variability and Sampling Requirements of the Visual Evaluation of Soil Structure in Cropped Fields." *Geoderma* 314: 58–62.
- Lin, L., J. De Pue, A. K. M. Vivanco, F. Van Der Bolt, and W. Cornelis. 2022. "Visual Assessment of Soil Structural Quality Across Soil Textures and Compaction Levels Part I: Examination of Intact Soil Cores." *Geoderma* 426: 116099.
- Manrique, L. A., and C. A. Jones. 1991. "Bulk Density of Soils in Relation to Soil Physical and Chemical Properties." *Soil Science Society of America Journal* 55: 476–481.

Nielsen, D. R., J. W. Biggar, and K. T. Erh. 1973. "Spatial Variability of Field-Measured Soil-Water Properties." *Hilgardia* 42: 215–259.

Perret, J., S. O. Prasher, A. Kantzas, and C. Langford. 1999. "Three-Dimensional Quantification of Macropore Networks in Undisturbed Soil Cores." *Soil Science Society of America Journal* 63: 1530–1543.

Poeplau, C., and A. Don. 2023. "A Simple Soil Organic Carbon Level Metric Beyond the Organic Carbon-To-Clay Ratio." *Soil Use and Management* 39: 1057–1067. https://doi.org/10.1111/sum.12921.

Prout, S., S. P. McGrath, G. J. D. Kirk, and S. M. Haefele. 2020. "What Is a Good Level of Soil Organic Matter? An Index Based on Organic Carbon to Clay Ratio." *European Journal of Soil Science* 72: 2493–2503. https://doi.org/10.1111/ejss.13012.

Rabot, E., N. P. A. Saby, M. P. Martin, et al. 2024. "Relevance of the Organic Carbon to Clay Ratio as a National Soil Health Indicator." *Geoderma* 443: 116829.

Rabot, E., M. Wiesmeier, S. Schlüter, and H.-J. Vogel. 2018. "Soil Structure as an Indicator of Soil Functions: A Review." *Geoderma* 314: 122–137.

Rowley, M. C., S. Grand, and É. P. Verrecchia. 2017. "Calcium-Mediated Stabilisation of Soil Organic Carbon." *Biogeochemistry* 137: 27–49. https://doi.org/10.1007/s10533-017-0410-1.

Sauzet, O., A. Johannes, C. Deluz, et al. 2024. "The Organic Carbon-To-Clay Ratio as an Indicator of Soil Structure Vulnerability, a Metric Focused on the Condition of Soil Structure." *Soil Use and Management* 40: e13060.

Schäffer, B., R. Schulin, and P. Boivin. 2008. "Changes in Shrinkage of Restored Soil Caused by Compaction Beneath Heavy Agricultural Machinery." *European Journal of Soil Science* 59: 771–783.

Schäffer, B., R. Schulin, and P. Boivin. 2013. "Shrinkage Properties of Repacked Soil at Different States of Uniaxial Compression." *Soil Science Society of America Journal* 77: 1930–1943.

Shabtai, I. A., R. C. Wilhelm, S. A. Schweizer, C. Höschen, D. H. Buckley, and J. Lehmann. 2023. "Calcium Promotes Persistent Soil Organic Matter by Altering Microbial Transformation of Plant Litter." *Nature Communications* 14: 6609.

Sisson, J. B., and P. J. Wierenga. 1981. "Spatial Variability of Steady-State Infiltration Rates as a Stochastic Process." *Soil Science Society of America Journal* 45: 699–704.

Vauclin, M., S. R. Vieira, R. Bernard, and J. L. Hatfield. 1982. "Spatial Variability of Surface Temerature Along Tow Transects of a Bare Soil." *Water Ressources Research* 18: 1677–1686.

Verrecchia, E. P., and L. Trombino. 2021. *A Visual Atlas for Soil Micromorphologists*. Springer International Publishing. https://doi.org/10.1007/978-3-030-67806-7.

Virto, I., R. Antón, M. Apesteguía, and A. Plante. 2018. "Role of Carbonates in the Physical Stabilization of Soil Organic Matter in Agricultural Mediterranean Soils." In *Soil Management and Climate Change*, 121–136. Elsevier.

Walkley, A., and I. A. Black. 1934. "An Examination of Degtjareff Method for Determining Soil Organic Matter and a Proposed Modification of the Chromic Acid Titration Method." *Soil Science* 1: 29–37.

Warkentin, B. P. 2008. "Soil Structure: A History From Tilth to Habitat." In *Advances in Agronomy*, 239–272. Academic Press.

World Reference Base for Soil Resources. 2022. World Reference Base for Soil Resources. 4th ed. International Union of Soil Sciences.

Young, I. M., and J. W. Crawford. 2004. "Interactions and Self-Organization in the Soil-Microbe Complex." *Science* 304: 1634–1637.

Yudina, A., and Y. Kuzyakov. 2023. "Dual Nature of Soil Structure: The Unity of Aggregates and Pores." *Geoderma* 434: 116478.

Zangiabadi, M., M. Gorji, M. Shorafa, S. Khavari Khorasani, and S. Saadat. 2020. "Effect of Soil Pore Size Distribution on Plant-Available Water and Least Limiting Water Range as Soil Physical Quality Indicators." *Pedosphere* 30: 253–262.

Supporting Information

Additional supporting information can be found online in the Supporting Information section. **Data S1-S4:** ejss70216-sup-0001-Supinfo.docx.